



# Brillouin optical time domain reflectometry for fast detection of dynamic strain incorporating double-edge technique

Mingjia Shangguan<sup>a,b,d</sup>, Chong Wang<sup>b</sup>, Haiyun Xia<sup>b,c,d,\*</sup>, Guoliang Shentu<sup>a,d</sup>, Xiankang Dou<sup>b</sup>, Qiang Zhang<sup>a,d,e</sup>, Jian-wei Pan<sup>a,d</sup>

<sup>a</sup> Shanghai Branch, National Laboratory for Physical Sciences at Microscale and Department of Modern Physics, USTC, Shanghai 201315, China

<sup>b</sup> CAS Key Laboratory of Geospace Environment, USTC, Hefei 230026, China

<sup>c</sup> Collaborative Innovation Center of Astronautical Science and Technology, HIT, Harbin 150001, China

<sup>d</sup> Synergetic Innovation Center of Quantum Information and Quantum Physics, USTC, Hefei 230026, China

<sup>e</sup> Jinan Institute of Quantum Technology, Jinan, Shandong 250101, China

## ARTICLE INFO

### Keywords:

Brillouin optical time-domain reflectometry  
Up-conversion technique  
Fabry-Perot interferometer

## ABSTRACT

For the first time, to the best of our knowledge, a direct detection Brillouin optical time-domain reflectometry (BOTDR) is demonstrated for fast distributed dynamic strain sensing incorporating double-edge technique, time-division multiplexing technique and upconversion technique. In order to guarantee the robust stability of the system, the double-edge technique is implemented by using a convert single-channel FPI and a fiber-coupled upconversion single-photon detector, incorporating a time-division multiplexing method. The upconversion single-photon detector is adopted to upconvert the backscattering photons from 1548.1 nm to 863 nm, which is subsequently detected by a Silicon avalanche photodiode (Si-APD). In the experiment, dynamic strain disturbance up to 1.9 mε over 1.5 km of a polarization maintaining fiber is detected at a sampling rate of 30 Hz. An accuracy of  $\pm 30 \mu\epsilon$  and spatial resolution of 0.6 m are realized.

## 1. Introduction

In the past two decades, Brillouin-based distributed optical fiber sensors have played an increasingly important role in various aspects of human life, such as large infrastructures, aerospace industry and geotechnical engineering [1]. The performance of distributed sensor based on Brillouin scattering has been improved significantly. Different techniques have been employed to distributed strain and temperature fiber sensors with high spatial resolution [2] or with long sensing range [3]. Recently, extensive research has been focused on developing distributed sensors for measurement of dynamic phenomena such as dynamic strain and sound wave.

The Brillouin-based distributed optical fiber dynamic strain sensor can mainly be divided into three types: the Brillouin optical time-domain analyzer (BOTDA), Brillouin optical correlation-domain analysis (BOCDA) and Brillouin optical time domain reflectometry (BOTDR).

The most widely used configuration is BOTDA. In BOTDA, a pulsed pump light and CW probe light with a frequency difference equivalent to the Brillouin frequency shift are launched at two opposite ends of the sensing fiber. The probe light at Stokes (anti-Stokes) frequency is

amplified (attenuated) by the pump light through the Brillouin gain (loss) process. By scanning the frequency of either the pump light or probe light, the Brillouin spectrum is obtained [4]. The conventional BOTDA (C-BOTDA) has been reported for dynamic strain sensor over 120 m at a sampling rate of 3.9 kHz with a spatial resolution of 12 m and strain resolution of 256  $\mu\epsilon$  [5]. However, in order to obtain the Brillouin gain spectrum, the conventional BOTDA requires that the frequency difference between the probe and pump signal should be scanned to cover the whole Brillouin spectrum. To overcome this problem, slope-assisted BOTDA (SA-BOTDA) and Brillouin phase-shift optical time domain analysis (BPS-OTDA) have been proposed. By using SA-BOTDA, a dynamic strain sensor along 85 m fiber at a repetition rate of 400 Hz with a spatial resolution of 1.5 m was demonstrated [6]. A precision of  $\pm 20 \mu\epsilon$  at 1.66 kHz sampling rate with 1 m resolution over a 160 m sensing fiber has been reported based on BPS-OTDA [7]. In BOTDA based on pulse pumping, spatial resolution is limited to 1 m due to the finite phonon lifetime. To overcome this constraint, several techniques including pulse pre-pump-BOTDA technique and differential pulse width pair technique have been proposed [1,8]. However, BOTDA is best reserved for monitoring single large disturbance, which induced Brillouin frequency

\* Corresponding author at: CAS Key Laboratory of Geospace Environment, USTC, Hefei 230026, China.

E-mail addresses: [hsia@ustc.edu.cn](mailto:hsia@ustc.edu.cn) (H. Xia), [dou@ustc.edu.cn](mailto:dou@ustc.edu.cn) (X. Dou), [qiangzh@ustc.edu.cn](mailto:qiangzh@ustc.edu.cn) (Q. Zhang).

shift is larger than the Brillouin bandwidth [9,10]. Otherwise, the Brillouin spectrum at a special point, from which one retrieves the strain and temperature information, is influenced by potential transfer of power between the pulsed pump light and the counterpropagating CW probe light in the fiber from the point where the pulse enters and the point under estimation. Note that, this effect can be neglected for short-range measurement, but significant for a long range distributed measurement [11].

The principle of the BOCDA is based on modulating the frequency or phase of two counter-propagating CW lights to invoke stimulated Brillouin scattering at one section of the sensing fiber at any given time [12]. The BOCDA shows unique features of random accessibility of measuring position, high spatial resolution and high speed [2]. By using the BOCDA, a dynamic strain measurement along a 100 m fiber at a repetition rate of 20 Hz with an accuracy of  $\pm 50 \mu\epsilon$  and a spatial resolution of about 80 cm have been demonstrated [13]. However, the sensing range in the classical BOCDA is about hundreds of the spatial resolution [2]. In order to enlarge the measurement range, additional time domain gating is demonstrated over 1 km sensing range with 7 cm spatial resolution [3]. But increasing the sensing range comes at the expense of achievable temporal resolution.

BOTDR is the simplest Brillouin-based technique, in which the variation of frequency and intensity of the spontaneous Brillouin backscatter signal is used to interrogate the temperature and strain along the sensing fiber [14]. Since the intensity of spontaneous Brillouin scattering is weak, it is challenging in developing a BOTDR with high temporal resolution. For example, by using a coherent-detection BOTDR (C-BOTDR), a maximum frequency of 2.5 Hz over 4 km sensing fiber has been demonstrated. However, the proposed system has a poor spatial resolution of 10 m [15]. In order to improve the spatial resolution and temporal resolution, a self-delayed heterodyne BOTDR (SDH-BOTDR) has been proposed and demonstrated along 1 km of sensing fiber with a spatial resolution of 1.5 m and a repetition rate of 25 Hz [16].

A direct-detection BOTDR (D-BOTDR) has been demonstrated by using an imbalanced Mach-Zhender interferometer (MZI), which is employed to convert the Brillouin frequency shift to intensity variation. A strain precision of  $\pm 50 \mu\epsilon$  over 2 km of sensing fiber with a spatial resolution of 1.3 m is demonstrated. However, the sampling rate is only 2 Hz [17]. The performances of typical Brillouin-based dynamic strain sensors are compared and listed in Table 1.

In our previous work, by using upconversion single-photon detector, a high spectral resolution BOTDR has been realized to detect the temperature profile over 9 km with spatial/temporal resolution of 2 m/15 s [18]. In this work, in order to fast detect of dynamic strain, a direct-detection BOTDR based on double-edge technique is used. The direct detection BOTDR incorporating up-conversion technique and double-edge technique has several advantages. Firstly, compared to InGaAs detector [17], up-conversion single-photon detector can detect Brillouin backscattering signal with higher quantum efficiency, lower noise and after pulse probability [19–21]. Secondly, the double-edge

technique is a common method to interrogate a small frequency shift, which has been demonstrated in Doppler wind LIDARS [22–24]. Finally, since the backscattering traces are recorded and averaged on a multiscaler (multiple-event time digitizer) in photon-counting acquisition mode (2-bit), the data volume is much smaller than the counterpart incoherent case (for example, a 14-bit analog to digital converter is used for sampling RF signal), and the photon-counting BOTDR can be operated for full raw data record and easy data recording.

## 2. Principle

The double-edge technique usually uses two edge filters with opposite slopes [22–24]. In this work, the transmission curve and reflection curve of the FPI are adopted to realize the double edges. Because of the symmetric arrangement of the double edges, the strain-induced Brillouin frequency shift will cause the signal to increase in one edge and to decrease in the other one. The variation of these two signals is sensitive to the change of the Brillouin spectrum, providing a unique detection scheme [25].

When a pulsed light launches into a sensing fiber, the power spectrum of the Brillouin backscatter  $S_B(\nu)$  is a convolution of the pulse spectrum  $S_p(\nu)$  and the Brillouin gain spectrum  $g_B(\nu)$ :

$$S_B(\nu) = S_p(\nu) \otimes g_B(\nu) \quad (1)$$

where  $\otimes$  denotes the convolution. Due to the exponential decay of the acoustic waves in the fiber core, the Brillouin gain spectrum  $g_B(\nu)$  has a Lorentzian spectral profile [26].

$$g_B(\nu) = g_0 [1 + (\nu - \nu_B)^2 / (w_B/2)^2] \quad (2)$$

where  $w_B$  is the full width at half-maximum (FWHM),  $\nu_B$  is the Brillouin shift,  $g_0$  is the peak value, given by

$$g_0 = 2\pi n_1^7 p_{12}^2 / c \lambda_p^2 \rho_0 V_a w_B \quad (3)$$

where  $n_1$  is the refractive index of the fiber,  $p_{12}$  is the longitudinal elastic-optic coefficient,  $c$  is the vacuum velocity of light,  $\lambda_p$  is the pump wavelength,  $\rho_0$  is the density,  $V_a$  is the acoustic velocity within the fiber.

In Eq. (12),  $\nu_B$  and  $w_B$  can be expressed as a linear function of temperature  $T$  and strain  $\epsilon$  as

$$\nu_B(T, \epsilon) = \nu_B(T_0, 0) + c_{\nu_B}^T (T - T_0) + c_{\nu_B}^\epsilon \epsilon \quad (4)$$

$$w_B(T, \epsilon) = w_B(T_0, 0) + c_{w_B}^T (T - T_0) + c_{w_B}^\epsilon \epsilon \quad (5)$$

where  $T_0$  is the reference temperature,  $c_{\nu_B}^T$ ,  $c_{w_B}^T$  and  $c_{\nu_B}^\epsilon$ ,  $c_{w_B}^\epsilon$  are the temperature and strain coefficients for the Brillouin shift and spectrum broadening.

In this work, the pulse spectrum  $S_p(\nu)$  can be approximated by a Gaussian function (this will be confirmed in the Experiment section), which can be expressed as:

$$S_p(\nu) = (\sqrt{\pi})^{-1} \exp[-(\nu - \nu_B)^2 / \Delta\nu_M^2] \quad (6)$$

**Table 1**

Performance chart of Brillouin-based dynamic strain sensors.

Figure of merit		Range	Sampling rate	Dynamic range	Spatial resolution	Strain precision	Reference
Detection scheme							
BOTDA	C-BOTDA	120 m	3.9 kHz	256 $\mu\epsilon$	12 m	–	[5]
	SA-BOTDA	85 m	0.4 kHz	600 $\mu\epsilon$	1.5 m	–	[6]
	BPS-OTDA	160 m	1.66 kHz	2.56 m $\epsilon$	1 m	$\pm 20 \mu\epsilon$	[7]
BOCDA	BOCDA	100 m	20 Hz	650 $\mu\epsilon$	0.8 m	$\pm 50 \mu\epsilon$	[13]
BOTDR	C-BOTDR	4 km	2.5 Hz	–	10 m	–	[15]
	SDH-BOTDR	1 km	25 Hz	–	1.5 m	–	[16]
	D-BOTDR(MZI)	2 km	2 Hz	10 m $\epsilon$	1.3 m	$\pm 50 \mu\epsilon$	[17]
	D-BOTDR(FPI)	1.5 km	30 Hz	2.4 m $\epsilon$	0.6 m	$\pm 30 \mu\epsilon$	this work

where  $\Delta\nu_M$  is the half-width at the 1/e intensity level of the pulse spectrum.

In order to eliminate the influence of the temperature on the measurement of the dynamic strain, the temperature profile along sensing fiber will be detected in advance. At a detected temperature  $T_D$ , the transmission of the Brillouin backscatter through the FPI varies with the strain of the sensing fiber experienced, which is given by

$$T_B(T_D, \epsilon) = \frac{\int_{-\infty}^{+\infty} S_B(\nu, T_D, \epsilon) h(\nu) d\nu}{\int_{-\infty}^{+\infty} S_B(\nu, T_D, \epsilon) d\nu} \quad (7)$$

where  $h(\nu)$  is the transmission function of the FPI. In this work, the cavity of the FPI is formed by two highly reflective multilayer mirrors that are deposited directly onto two carefully aligned fiber ends. The anti-reflection coated fiber inserted in the cavity provides confined light-guiding and eliminates secondary cavity. Since the FPI is fabricated with single-mode fiber with a negligible divergence in the cavity, its transmission is approximated to a Lorentzian function:

$$h(\nu) = T_M/[1 + \nu^2/(\Delta\nu_{FPI}/2)^2] \quad (8)$$

where  $\Delta\nu_{FPI}$  is the FWHM of the transfer function,  $T_M$  is the maximum transmission factor given by:

$$T_M = a_t(1 - r_f)^2/(1 - a_t r_f)^2 \quad (9)$$

where  $a_t$  is the attenuation factor,  $r_f$  is the reflection coefficient of the reflecting ends.

For the purpose of improving the sensitivity of strain measurement and making full use of the Brillouin backscatter, the reflected signal of the Brillouin backscatter on the FPI is detected simultaneously, which can be expressed as:

$$R_B(T_D, \epsilon) = \frac{\int_{-\infty}^{+\infty} S_B(\nu, T_D, \epsilon) r(\nu) d\nu}{\int_{-\infty}^{+\infty} S_B(\nu, T_D, \epsilon) d\nu} \quad (10)$$

where  $r(\nu) = 1 - h(\nu)$  is the reflection function of the FPI.

Then, a response function is defined as

$$Q(T_D, \epsilon) = \frac{a_0 T_B(T_D, \epsilon) - R_B(T_D, \epsilon)}{a_0 T_B(T_D, \epsilon) + R_B(T_D, \epsilon)} \quad (11)$$

where  $a_0$  is a system constant, which can be determined in the calibration.

The operating principle of the double-edge is shown in Fig. 1(a). The double-edge technique is implemented by making use of the transmission curve and reflection curve of the FPI. As shown in Eqs. (4) and (5), the strain not only affects the Brillouin frequency shift but also the bandwidth of the Brillouin gain spectrum, which leads to complement variations of the transmitted signal and reflected signal on the FPI. As shown in Fig. 1(b), with the known temperature and strain coefficients and temperature value (these coefficients can be found in Experiment section), the response function  $Q$  varies monotonically with the strain that the sensing fiber experienced. In this work, a demonstrated experiment is carried out in the lab at temperature of 25 °C. The strain ranging from 0.7 mε to 1.9 mε is marked between two red points, as shown in Fig. 1(b).

### 3. Instrument

A schematic diagram of the direct-detection BOTDR is shown in Fig. 2. The laser adopts master oscillator power amplifier structure. The CW laser from a distributed feedback diode (DFB, 1548.1 nm) is chopped into a pulse train by using an electro-optic modulator (EOM<sub>1</sub>, Photline, MXER-LN-10). The EOM<sub>1</sub> is driven by using a pulse generator, which determines the shape and period of the laser pulse. The period of the pulses is set to 32 μs, which indicates a maximum unambiguous detection range of 3.2 km. The output pulse is amplified by an erbium-doped fiber amplifier (EDFA). The CW leakage is further

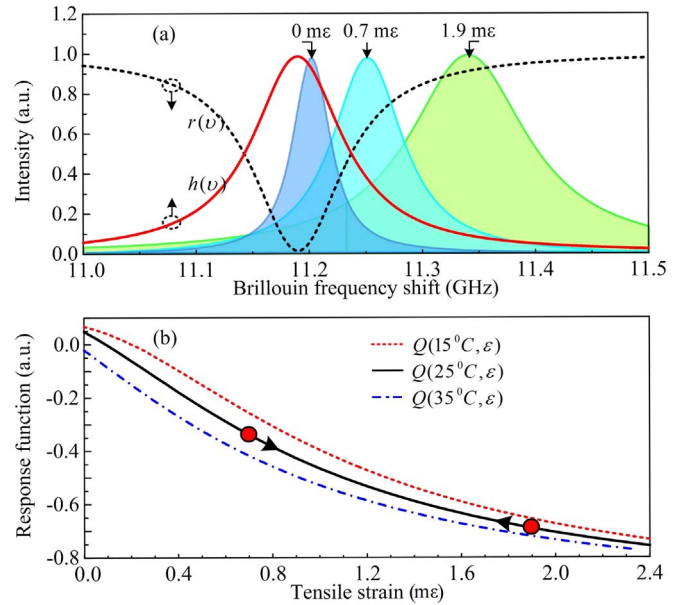


Fig. 1. (a) The transmission curve and reflection curve of the FPI, and the Brillouin gain spectra when the sensing fiber experiences different strains at the temperature of 25 °C; (b) response functions versus the tensile strain when the fiber experiences different temperatures.

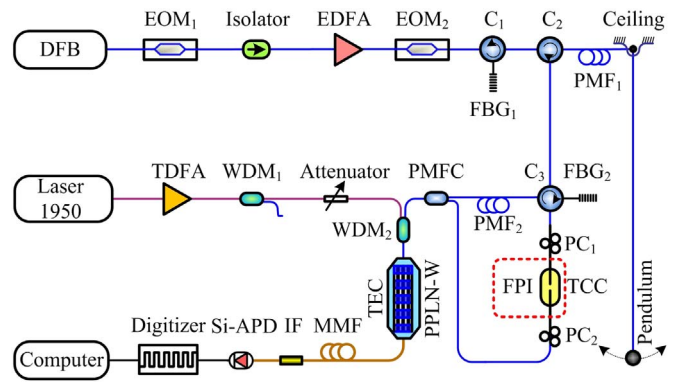


Fig. 2. Optical layout of the system. DFB, distributed feedback diode; EOM, electro-optic modulator; EDFA, erbium doped fiber amplifier; C, circulator; FBG, fiber Bragg grating; PMF, polarization-maintaining fiber; PC, polarization controller; FPI, Fabry-Perot interferometer; TCC, temperature controlled chamber; PMFC, polarization-maintaining fiber coupler; TDFA, thulium doped fiber amplifier; WDM, wavelength division multiplexer; PPLN-W, periodically poled Lithium niobate waveguide; TEC, thermo-electric cooler; MMF, multimode fiber; IF, interferometer filter.

suppressed to -50 dB with another EOM<sub>2</sub>, which minimizes the amplified spontaneous emission (ASE) in the EDFA simultaneously. The ASE is further filtered by inserting a fiber Bragg grating (FBG<sub>1</sub>) with ultra-narrow band of 6 pm. The filtered pulses are launched into the sensing fiber. The peak power of the pulse is 21 dBm. The sensing fiber comprised 1.5 km of unstrained polarization-maintaining fiber (PMF<sub>1</sub>) with 1.8 m of strained fiber at the rear end. Since the FPI and the up-conversion detector are both polarization sensitive devices, a PMF is used in this work instead of a single-mode fiber to mitigate the polarization fading problem. If a single-mode fiber is used, a polarization scrambler should be added and the signal to noise ratio will be reduced. A brass ball with the weight of 110 g is suspended at the end of the 1.8 m fiber, forming a pendulum. The 1.8 m strained region is isolated by using glue. When the pendulum oscillates about the equilibrium position, the strain of the sensing fiber experienced changes periodically.

The Stokes Brillouin backscatter signal (BBS) is picked out against the strong Rayleigh backscatter component by using a FBG<sub>2</sub> with

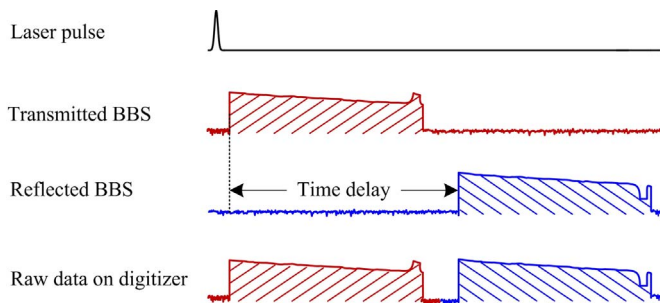


Fig. 3. Timing sequence of data acquisition for a single laser pulse.

bandwidth of 6 pm. The FPI is used as the frequency discriminator. Because the FPI is made of single-mode fiber, two polarization controllers (PC) are added at the front and rear ends of the FPI to eliminate the polarization-dependent loss. To guarantee the system stability, the FPI is cased in a temperature-controlled chamber (TCC).

As shown in Fig. 3, the transmitted signal of the Brillouin backscatter through the FPI is directed into an upconversion detector, while the reflected Brillouin backscatter signal is timely delayed through a circulator ( $C_3$ ) and 3.2 km PMF<sub>2</sub>. After passing a polarization-maintaining fiber coupler (PMFC), the transmitted and reflected Brillouin backscatter signals are directed into the detector alternatively.

The CW wave from the pump laser at 1950 nm is followed by a thulium-doped fiber amplifier (TDFA), which amplified the power of the pump laser up to 400 mW. The residual ASE noise is suppressed by using a 1.55/1.95  $\mu\text{m}$  wavelength division multiplexer (WDM<sub>1</sub>). The Brillouin backscatter signal and the pump laser are coupled into a periodically poled lithium niobate waveguide (PPLN-W) via a WDM<sub>2</sub>. It optimized quasi-phase matching condition is achieved by tuning the temperature of the PPLN-W with a thermoelectric cooler [27]. Here, the upconversion detector is integrated into an all-fiber module, in which the PPLN-W is coupled into a PMF/multimode fiber (MMF) at the front/rear end. The backscatter photons at 1548.1 nm are converted into sum-frequency photons at 863 nm and then picked out from the pump and spurious noise by using an interferometer filter (IF) at 863 nm with bandwidth of 1 nm. Finally, the photons at 863 nm are detected by a Si-APD. The TTL signals corresponding to the received photons are recorded on a digitizer and then transferred into a computer. Even though the conversion efficiency can approach a value larger than 99%, due to the coupling losses, the attenuation of the PPLN-W, and the limited quantum efficiency of the Si-APD at 863 nm, the final system efficiency of the UPD is 20% with a noise of 300 counts per second.

#### 4. Experiment

Because the spatial resolution is determined by the width of a launched pulse, a short light pulse is required to improve the spatial resolution. As the pulse width becomes shorter, the bandwidth of the spectrum of Brillouin backscatter broadens, which leads to a larger dynamic range of the strain measurement. However, it will also result in the decreasing of the measurement sensitivity [28]. In this work, considering the trade-off between the spatial resolution and the measurement accuracy, a pulse light with the FWHM of 6 ns is used, which corresponds to the spatial resolution of 0.6 m according to the equation  $\Delta R = c\tau/2$  ( $\Delta R$  is the spatial resolution,  $c$  is the speed of light inside fiber,  $\tau$  is the FWHM of the laser pulse). Fig. 4(a) presents the measured pulse in the time domain and transformed into the frequency domain, and Fig. 4(b) shows the output spectrum of the laser. A fast Fourier transform (FFT) is carried out with 502 points and sample-rate of 2.5 GSa/s. The result and its Gaussian fitting curve are shown as the inset in Fig. 4(a). The fitted bandwidth of the pulse shape in the frequency domain is 73.2 MHz, which agrees with  $\Delta\nu\Delta t=0.44$ , indicating a transform limited optical pulse ( $\Delta\nu/\Delta t$  is the temporal/ spectral

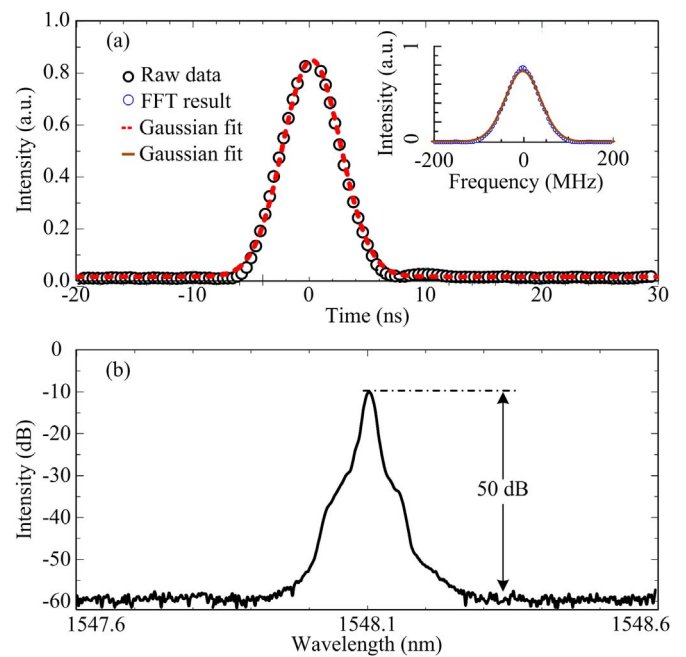


Fig. 4. (a): The pulse shape in time domain and in frequency domain (inset figure, obtain by Fourier transform of time profile of pulse), (b): the output spectrum of the laser.

width). As shown in Fig. 4(a), the assumption that the pulse spectrum is Gaussian function as shown in Eq. (12) is confirmed.

In a calibration experiment, a scheme of high spectral resolution BOTDR is adopted, which has been described in detail elsewhere [18]. In the FPI, a stacked piezoelectric transducer is used to axially strain the single-mode fiber inserted into the cavity. Frequency scanning of the FPI is achieved by scanning the cavity length.

As shown in Fig. 5(a), the transmission and reflection curves, from monochromatic CW laser, the laser pulse and BBS are obtained by scanning the FPI over 600 MHz with a step of 15 MHz. By using the nonlinear fitting method, the response functions of CW laser (indicated by  $Q_{CW}$ ), the laser pulse (indicated by  $Q_{Pulse}$ ) and BBS (indicated by  $Q_{BBS}$ ) are calculated as shown in Fig. 5(b) and compared in Fig. 5(d). The fitting residuals relative to the peaks are also provided for monitoring of the data quality, as shown in Fig. 5(c). Since the linewidth of the monochromatic CW laser ( $\approx 3$  kHz) is much less than that of the FPI, the measured spectrum represents the feature of the FPI. The fitting bandwidth of  $Q_{CW}$  is 94 MHz. The fitted bandwidth of the response function of  $Q_{BBS}$  is 180 MHz, which corresponds to the dynamic range of about 2.4  $\text{m}\epsilon$ .

By applying various strains on the sensing fiber at a constant temperature, the measured response functions are obtained. And then the nonlinear fitting method is performed to fit the calculated response functions to Voigt function. To gather statistics of the fitted Brillouin frequency shifts and spectrum broadenings at different strain, the strain coefficients are measured  $c_{FB}^{\epsilon}=0.075$  MHz/ $\mu\epsilon$  and  $c_{wB}^{\epsilon}=0.05$  MHz/ $\mu\epsilon$ . Similarly, applying various temperatures on the unstrained sensing fiber, the temperature coefficients are measured  $c_{FB}^T=1.46$  MHz/ $^{\circ}\text{C}$  and  $c_{wB}^T=0.15$  MHz/ $^{\circ}\text{C}$ . These parameters are used for calculating the response curve as shown in Fig. 1(b). Note that, the transmission and reflection curve of the BBS on the FPI in Fig. 5(a–3) is measured when the sensing fiber is free of strain and at the temperature of 25  $^{\circ}\text{C}$ .

When the pendulum is displaced sideways from its resting (equilibrium position), it is subject to a restoring force due to gravity that will accelerate it back toward the equilibrium position. After released, the restoring force will make the brass ball oscillate about the equilibrium position, swinging back and forth. As the pendulum swings, the strain

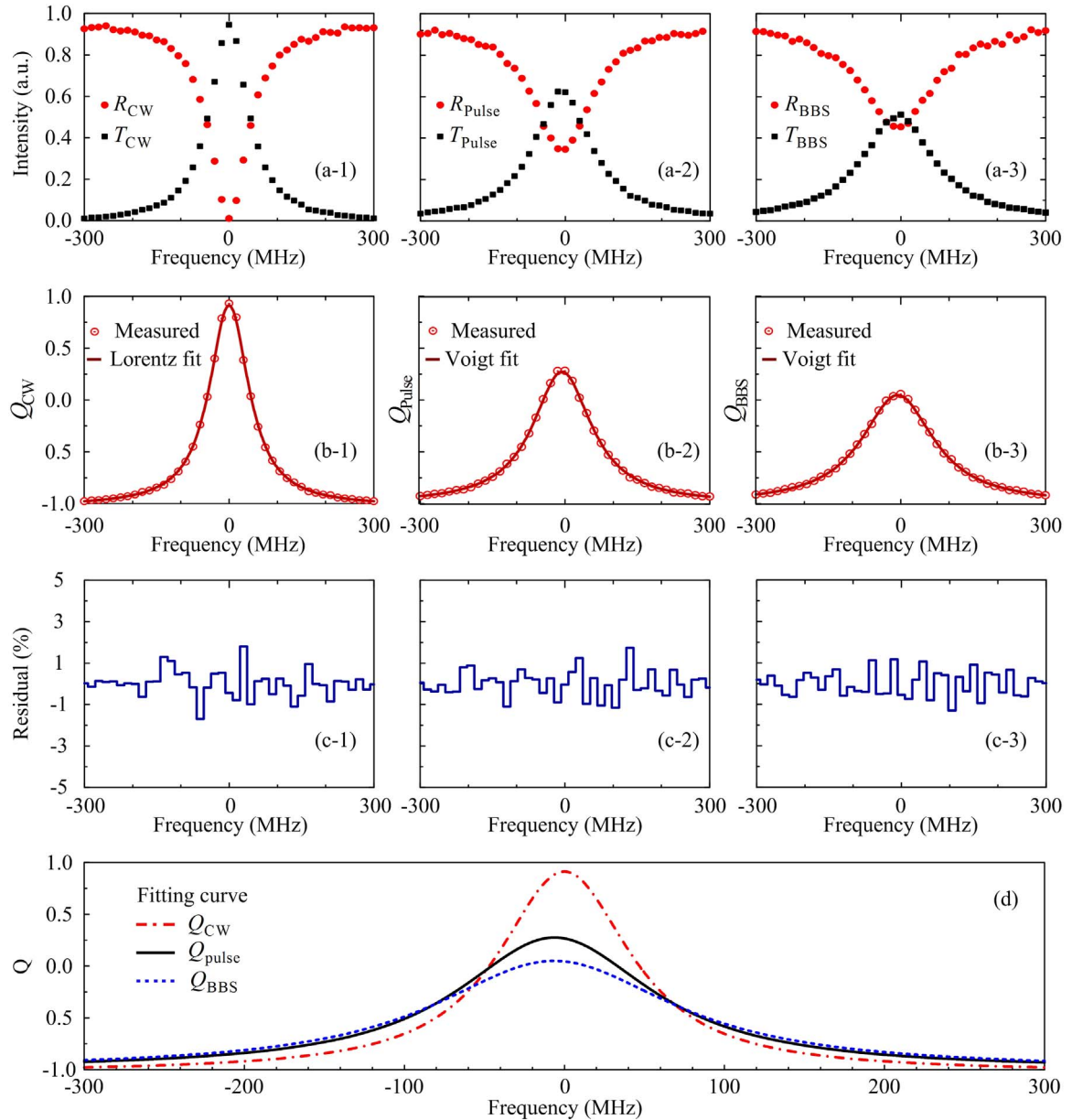


**Fig. 5.** (a) Transmission and reflection curves of a monochromatic CW laser (a-1, indicated by  $T_{CW}$  and  $R_{CW}$ ), the laser pulse with bandwidth of 6 ns (a-2, indicated by  $T_{Pulse}$  and  $R_{Pulse}$ ), and Brillouin backscatter of the laser with bandwidth of 6 ns (a-3, indicated by  $T_{BBS}$  and  $R_{BBS}$ ) by scanning the cavity length of the FPI, (b) the measured response functions and its nonlinear fitting result, (c) residuals between the measured response functions and its fitting results, which are relative to the peak, (d) comparison among three fitting curves.

of the sensing fiber experienced changes periodically. And the period of the simple pendulum can be expressed as [29]:

$$P = 2(2L/g)^{1/2} \int_0^{\theta_0} 1/(\cos \theta - \cos \theta_0)^{1/2} d\theta \quad (12)$$

where  $L$  is the length of the sensing fiber,  $g$  is the local acceleration of gravity,  $\theta_0$  is the maximum angle that the pendulum swings away from vertical position (in experience,  $\theta_0 = 55^\circ$ ).

As the pendulum swings, the tension of the sensing fiber shows the sinusoidal nature, as shown in Fig. 6(a). The sampling rate of the digitizer is 500 MSa/s, which corresponds to one sample every 0.2 m. In order to match the bandwidth (6 ns) of the laser pulse, a three-point average is performed, which leads to the spatial resolution of 0.6 m. The Brillouin backscatter signals from 1042 laser pulses are accumulated, which corresponds to the sampling rate of 30 Hz. The measured results are fit to a sine function by applying a least-square fit based on Levenberg-Marquardt algorithm, as shown in Fig. 6(a). The measured period of the pendulum is 2.88 s, which is close to the theoretical value

of 2.86 s ( $g=9.795 \text{ m/s}^2$  at Hefei (31.843°N, 117.265°E), China) calculated by using Eq. (12). The measured period of the pendulum is slightly larger than the calculated one. This phenomenon may be mainly due to two reasons. Firstly, the stretch of the sensing fiber will increase the period of the pendulum. Secondly, air resistance will also slow down the pendulum since the brass ball has a diameter of 32 mm. The histogram distribution of the strain difference between the measured results and fitting results is shown in Fig. 6(b). The Gaussian fitting result is shown by the dash line superimposed on the histogram. The mean difference is  $1 \mu\epsilon$ . The half width at half maximum (HWHM) is  $30 \mu\epsilon$ , which means the precession of this method can be reached to  $\pm 30 \mu\epsilon$ .

## 5. Conclusion

A direct detection BOTDR has been demonstrated for distributed dynamic strain sensing incorporating double-edge technique, time-division multiplexing technique and upconversion technique. The

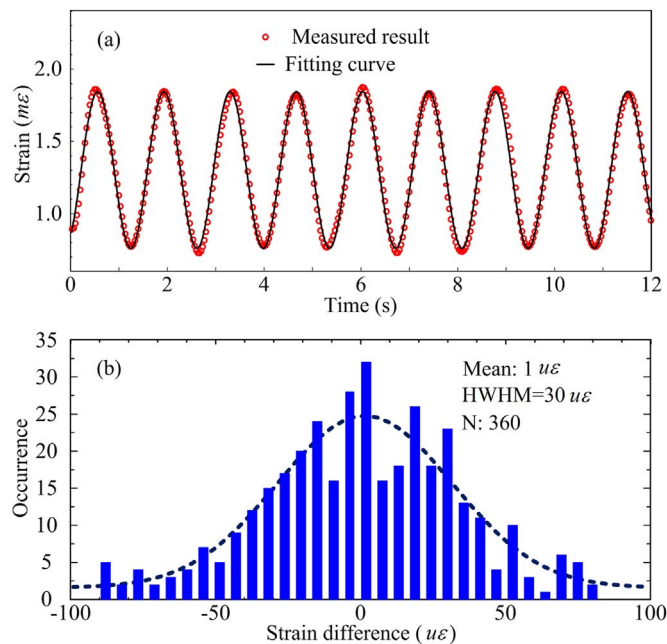


**Fig. 6.** (a) Retrieved strain results; (b) histogram distribution of the strain difference between the measured result and fitting result.

double edges are realized by using the transmission curve and reflection curve of an all-fiber FPI. Benefiting from the low insert loss of the fiber at  $1.5 \mu\text{m}$ , the time-division multiplexing technique is performed to realize the double-edge only using one single-channel FPI and one detector, which improve the system accuracy and stability substantially. By using upconversion technique, a high signal-to-noise upconversion detector is used to detect the weak spontaneous Brillouin backscatter signal efficiently. In demonstrated experiment, dynamic strain disturbance up to  $1.9 \text{ m}\epsilon$  over the  $1.5 \text{ km}$  is detected at a sampling rate of  $30 \text{ Hz}$  with an accuracy of  $\pm 30 \mu\epsilon$  and spatial resolution of  $0.6 \text{ m}$ .

## References

- [1] C.A. Galindex-Jamioy, J.M. Lopez-Higuera, Brillouin distributed fiber sensors: an overview and applications, *J. Sens.* (2012) (204121).
- [2] K.Y. Song, Z. He, K. Hotate, Distributed strain measurement with millimeter-order spatial resolution based on Brillouin optical correlation domain analysis, *Opt. Lett.* 31 (2006) 2526–2528.
- [3] K. Hotate, H. Arai, K.Y. Song, Range-enlargement of simplified Brillouin optical correlation domain analysis based on a temporal gating scheme, *SICE J. Cont. Meas. Syst. Integr.* 1 (2008) 271–274.
- [4] T. Kurashima, T. Horiguchi, M. Tateda, Distributed-temperature sensing using stimulated Brillouin scattering in optical silica fibers, *Opt. Lett.* 15 (1990) 1038–1040.
- [5] P. Chaube, B.G. Colpitts, D. Jagannathan, A.W. Brown, Distributed fiber-optic sensor for dynamic strain measurement, *IEEE Sens. J.* 8 (2008) 1067–1072.
- [6] Y. Peled, A. Motil, L. Yaron, M. Tur, Slope-assisted fast distributed sensing in optical fibers with arbitrary Brillouin profile, *Opt. Express* 19 (2011) 19845–19854.
- [7] J. Urricelqui, A. Zornoza, M. Sagues, A. Loayssa, Dynamic BOTDA measurements based on Brillouin phase-shift and RF demodulation, *Opt. Express* 20 (2012) 26942–26949.
- [8] K. Kishida, C. Li, Pulse pre-pump-BOTDA technology for new generation of distributed strain measuring system. In *Structural Health Monitoring And Intelligent Infrastructure*, 2005, 471–477.
- [9] T.R. Parker, M. Farhadiroushan, R. Fececi, V.A. Handerek, Simultaneous distributed measurement of strain and temperature from noise-initiated Brillouin scattering in optical fibers, *Quantum Electron.* 34 (1998) 645–659.
- [10] T. Horiguchi, K. Shimizu, T. Kurashima, M. Tateda, Y. Koyamada, Development of a distributed sensing technique using Brillouin scattering, *J. Light. Technol.* 13 (1995) 1296–1302.
- [11] L. Thvenaz, S.F. Mafang, J. Lin, Effect of pulse depletion in a Brillouin optical time-domain analysis system, *Opt. Express* 21 (2013) 14017–14035.
- [12] K. Hotate, Fiber distributed Brillouin sensing with optical correlation domain techniques, *Opt. Fiber Technol.* 19 (2013) 700–719.
- [13] K.Y. Song, M. Kishi, Z. He, K. Hotate, High-repetition-rate distributed Brillouin sensor based on optical correlation-domain analysis with differential frequency modulation, *Opt. Lett.* 36 (2011) 2062–2064.
- [14] H.H. Kee, G.P. Lees, T.P. Newson, All-fiber system for simultaneous interrogation of distributed strain and temperature sensing by spontaneous Brillouin scattering, *Opt. Lett.* 25 (2000) 695–697.
- [15] F. Wang, X. Zhang, X. Wang, H. Chen, Distributed fiber strain and vibration sensor based on Brillouin optical time-domain reflectometry and polarization optical time-domain reflectometry, *Opt. Lett.* 38 (2013) 2437–2439.
- [16] K. Koizumi, Y. Kanda, A. Fujii, and H. Murai, High-speed distributed strain measurement using Brillouin optical time-domain reflectometry based on self-delayed heterodyne detection, *IEEE European Conference on*, 2015, 1–3.
- [17] A. Masoudi, M. Belal, T.P. Newson, Distributed dynamic large strain optical fiber sensor based on the detection of spontaneous Brillouin scattering, *Opt. Lett.* 38 (2013) 3312–3315.
- [18] H. Xia, M. Shangguan, G. Shentu, C. Wang, J. Qiu, M. Zheng, X. Xie, X. Dou, Q. Zhang, J.W. Pan, Brillouin optical time-domain reflectometry using up-conversion single-photon detector, *Opt. Commun.* 381 (2016) 37–42.
- [19] E. Diamanti, C. Langrock, M.M. Fejer, Y. Yamamoto, H. Takesue, 1.5 m photon-counting optical time-domain reflectometry with a single-photon detector based on upconversion in a periodically poled lithium niobate waveguide, *Opt. Lett.* 31 (2006) 727–729.
- [20] H. Xia, G. Shentu, M. Shangguan, X. Xia, X. Jia, C. Wang, J. Zhang, J.S. Pelc, M.M. Fejer, Q. Zhang, X. Dou, J.W. Pan, Long-range micro-pulse aerosol lidar at  $1.5 \text{ m}$  with an upconversion single-photon detector, *Opt. Lett.* 40 (2015) 1579–1582.
- [21] M. Shangguan, H. Xia, C. Wang, J. Qiu, G. Shentu, Q. Zhang, X. Dou, J.W. Pan, All-fiber upconversion high spectral resolution wind lidar using a Fabry-Perot interferometer, *Opt. Express* 24 (2016) 19322–19336.
- [22] H. Xia, D. Sun, Y. Yang, F. Shen, J. Dong, T. Kobayashi, Fabry-Perot interferometer based Mie Doppler lidar for low tropospheric wind observation, *Appl. Opt.* 46 (2007) 7120–7131.
- [23] H. Xia, X. Dou, D. Sun, Z. Shu, X. Xue, Y. Han, D. Hu, Y. Han, T. Cheng, Mid-altitude wind measurements with mobile Rayleigh Doppler lidar incorporating system-level optical frequency control method, *Opt. Express* 20 (2012) 15286–15300.
- [24] H. Xia, M. Shangguan, C. Wang, G. Shentu, J. Qiu, Q. Zhang, X. Dou, J.W. Pan, Micro-pulse upconversion Doppler lidar for wind and visibility detection in the atmospheric boundary layer, *Opt. Lett.* 41 (2016) 5218–5221.
- [25] H. Xia, C. Zhang, H. Mu, D. Sun, Edge technique for direct detection of strain and temperature based on optical time domain reflectometry, *Appl. Opt.* 48 (2009) 189–197.
- [26] D. Heiman, D.S. Hamilton, R.W. Hellwarth, Brillouin scattering measurements on optical glasses, *Phys. Rev. B.* 19 (1979) 6583–6589.
- [27] G. Shentu, J.S. Pelc, X. Wang, Q. Sun, M. Zheng, M.M. Fejer, Q. Zhang, J. Pan, Ultralow noise up-conversion detector and spectrometer for the telecom band, *Opt. Express* 21 (2013) 13986–13991.
- [28] H. Naruse, M. Tateda, Trade-off between the spatial and the frequency resolutions in measuring the power spectrum of the Brillouin backscattered light in an optical fiber, *Appl. Opt.* 38 (1999) 6516–6521.
- [29] F.M.S. Lima, P. Arun, An accurate formula for the period of a simple pendulum oscillating beyond the small angle regime, *Am. J. Phys.* 74 (2006) 892–895.